Dilute Surfactant Methods for Carbonate Formations

ID Number: DE-FC26-02NT 15322

Quarterly Progress Report

Reporting Period Start Date: 7-1-2005

Reporting Period End Date: 9-30-2005

Submitted to the

U.S. Department of Energy

Kishore K. Mohanty

Department of Chemical Engineering

University of Houston

4800 Calhoun Road

Houston, Texas 77204-4004

October, 2005

Disclaimer

Abstract

There are many carbonate reservoirs in US (and the world) with light oil and fracture pressure below its minimum miscibility pressure (or reservoir may be naturally fractured). Many carbonate reservoirs are naturally fractured. Waterflooding is effective in fractured reservoirs, if the formation is water-wet. Many fractured carbonate reservoirs, however, are mixed-wet and recoveries with conventional methods are low (less than 10%). Thermal and miscible tertiary recovery techniques are not effective in these reservoirs. Surfactant flooding (or huff-n-puff) is the best hope, yet it was developed for sandstone reservoirs in the past. The goal of this research is to evaluate dilute (hence relatively inexpensive) surfactant methods for carbonate formations and identify conditions under which they can be effective. Laboratory-scale surfactant brine imbibition experiments give high oil recovery (35-62% OOIP) for initially oil-wet cores through wettability alteration and IFT reduction. Core-scale simulation results match those of the experiments. Initial capillarity-driven imbibition gives way to a final gravity-driven process. As the matrix block height increases, surfactant alters wettability to a lesser degree, or permeability decreases, oil production rate decreases. The scale-up to field scale will be further studied in the next quarter.

TABLE OF CONTENTS

List of Graphical Materials

Executive Summary

There are many carbonate reservoirs in US (and the world) with light oil and fracture pressure below its minimum miscibility pressure (or reservoir may be naturally fractured). Many carbonate reservoirs are naturally fractured. Waterflooding is effective in fractured reservoirs, if the formation is water-wet. Many fractured carbonate reservoirs, however, are mixed-wet and recoveries with conventional methods are low (less than 10%). Thermal and miscible tertiary recovery techniques are not effective in these reservoirs. Surfactant flooding (or huff-n-puff) is the best hope, yet it was developed for sandstone reservoirs in the past. The goal of this research is to evaluate dilute (hence relatively inexpensive) surfactant methods for carbonate formations and identify conditions under which they can be effective. Laboratory-scale surfactant brine imbibition experiments give high oil recovery (35-62% OOIP) for initially oil-wet cores through wettability alteration and IFT reduction. Core-scale simulation results match those of the experiments. Initial capillarity-driven imbibition gives way to a final gravity-driven process. As the matrix block height increases, surfactant alters wettability to a lesser degree, or permeability decreases, oil production rate decreases. The scale-up to field scale will be further studied in the next quarter.

Introduction

There are many carbonate reservoirs in US (and the world) with light oil and fracture pressure below its minimum miscibility pressure (or reservoir may be naturally fractured). Many carbonate reservoirs are naturally fractured. Waterflooding is effective in fractured reservoirs, if the formation is water-wet. Many fractured carbonate reservoirs, however, are mixed-wet and recoveries with conventional methods are low (less than 10%). Thermal and miscible tertiary recovery techniques are not effective in these reservoirs. Surfactant flooding (or huff-n-puff) is the only hope,[1] yet it was developed for sandstone reservoirs in the past.[2]

The goal of this research is to evaluate dilute surfactant methods for carbonate formations and identify conditions under which they can be effective. Adsorption, phase behavior, wettability alteration, IFT gradient driven imbibition, blob mobilization at high capillary and Bond numbers will be quantified. An existing laboratory simulator will be modified to incorporate the mechanisms of surfactant transport and effective parameters will be developed to model this process in a dual porosity reservoir simulator. Field-scale simulations will be conducted to identify criteria under which dilute surfactant methods are feasible without active mobility control.

This report summarizes our results for the period of January, 2005 through April, 2005. The five tasks for the project are: (1) Adsorption, (2) Wettability alteration, (3) Gravity and viscous mobilization, (4) Imbibition, and (5) Simulation. The fifth task was worked on this quarter and is highlighted in this report.

Experimental

Limestone cores (6" long, 1.5" diameter) were saturated with 100% field brine and then displaced with crude oil to residual water saturation (27.5%). The cores were then aged in an oil bath for a period of 18 days (or more), to make it oil wet in nature. The cores were then used in imbibition cells filled with brine containing 0.05 wt % surfactant and 0.3 M Na_2CO_3. The single-phase brine permeability was about 150 md, and the initial oil saturation was about 72.5%. The ratio of the total amount of water in the imbibition cell and core to the amount of oil is approximately 10.

Modeling Methods

The effect of alkaline surfactant solution on oil production from an oil-wet fracture block is studied with a 3-D numerical simulator. The capillary pressure between oil and brine phase, the relative permeabilities and the residual saturation of both phases are considered as functions of IFT and wettability. These are in turn correlated to the surfactant and salt concentrations with the data obtained from laboratory experiments.

Phase behavior. The study is based on an isothermal system. Four components are considered: hydrocarbon, water, surfactant and salt. It is assumed that the overall surfactant concentration is low, less than 0.1 wt%. Experiments[3] indicate that the amount of the third micro-emulsion phase is small; so we consider only two fluid phases: oil phase and aqueous phase. Based on this assumption, the following equation must be satisfied:

$$S_a + S_o = 1 \qquad (1)$$

where the subscript "a" represents the aqueous phase and "o" represents the oil phase. S_j is the saturation of phase *j* (j=a,o).

According to the experimental observations,[3] the following assumptions are made regarding the distribution of components among different phases:

- Hydrocarbon can exist in oil phase and aqueous phase;
- Water can exist in aqueous phase and oil phase;
- Surfactant can exist in aqueous phase and oil phase, and on the solid surface;
- Salt can exist in aqueous phase and can be absorbed onto matrix surface.

Based on these assumptions, the mass balances at any position can be described with:

$$w_a^w + w_a^h + w_a^{sf} + w_a^{st} = 1 \qquad (2a)$$

$$w_o^w + w_o^h + w_o^{sf} = 1 \qquad (2b)$$

$$\phi C^{sf} = \phi\left(\rho_a S_a w_a^{sf} + \rho_o S_o w_o^{sf}\right) + A_s C_r^{sf} \qquad (2c)$$

$$\phi C^{st} = \phi \rho_a S_a w_a^{st} + A_s C_r^{st} \qquad (2d)$$

where, the superscript "w" represents the water component, "h" represents the hydrocarbon component, "sf" represents the surfactant and "st" refers to the salt component. ϕ is the porosity; ρ_j is the density of phase j; w_j^i is the mass fraction of component i in phase j; C^{sf} and C^{st} (kg/m^3) are overall concentrations of surfactant and salt in kg per unit volume; C_r^{sf} and C_r^{st} (kg/m^2) are the concentrations of surfactant and salt absorbed on matrix surface in kg per unit area; A_s is the specific matrix surface area (m^2/m^3 matrix).

For a local site in the medium, if the matrix properties (ϕ and A_s), the phase densities (ρ_j), either of the phase saturations (S_o in this study) and the overall concentrations of surfactant and salt (C^{sf} and C^{st}) are given, there are 10 unknowns in Eqs. (1) and (2a) – (2d): $S_a, w_a^w, w_a^h, w_a^{sf}, w_a^{st}, w_o^w, w_o^h, w_o^{sf}, C_r^{sf}$ and C_r^{st}. Local equilibrium is assumed for the distribution of any component among different phases. Under this assumption, Eqs. (1) and (2a) – (2d) are

closed by the phase diagram, which determines the partition of each component among the aqueous phase, oil phase and matrix phase. In this work, the following correlations are needed:

$$w_a^h = w_a^h\left(C^{sf}, C^{st}, S_o, \rho_o, S_a, \rho_a, \phi, A_s\right) \qquad (3a)$$

$$w_a^{sf} = w_a^{sf}\left(C^{sf}, C^{st}, S_o, \rho_o, S_a, \rho_a, \phi, A_s\right) \qquad (3b)$$

$$w_a^{st} = w_a^{st}\left(C^{sf}, C^{st}, S_o, \rho_o, S_a, \rho_a, \phi, A_s\right) \qquad (3c)$$

$$w_o^w = w_o^w\left(C^{sf}, C^{st}, S_o, \rho_o, S_a, \rho_a, \phi, A_s\right) \qquad (3d)$$

$$w_o^{sf} = w_o^{sf}\left(C^{sf}, C^{st}, S_o, \rho_o, S_a, \rho_a, \phi, A_s\right) \qquad (3e)$$

For a certain system, the correlations described by Eqs. (3a) – (3e) can be determined from experimental data. From these five correlations along with Eqs. (1) and (2a) – (2d), the distribution of each component among different phases can be determined. The effect of pressure on density is incorporated by considering the compressibility of oil phase:

$$\rho_o = \rho_o^0 + \beta\left(p_o - 101325\right) \qquad (4)$$

where ρ_o^0 is the oil density at 1 atmosphere (101,325Pa) and β is the compressibility of oil. The values of ρ_o^0 and β are dependent on the type of oil. The aqueous phase is assumed to be incompressible.

Mass transfer models. In this study, we neglect the effect of hydraulic dispersion and assume that the overall mass flux of each component is a linear summation of convection and molecular diffusion:[4]

$$\overline{F}_i = \rho_a \bar{v}_a w_a^i + \rho_o \bar{v}_o w_o^i - D_a^{i,e} \nabla w_a^i - D_o^{i,e} \nabla w_o^i \qquad (5)$$

The phase velocity, $\bar{v}_j$ is determined from Darcy's law:

$$\bar{v}_j = -\frac{k_{rj}}{\mu_j}\bar{\bar{K}} \cdot \left(\nabla p_j + \rho_j \bar{g}\right) \quad . \tag{6}$$

Here $\bar{\bar{K}}$ is the absolute permeability tensor; k_{rj} is the relative permeability of phase j; μ_j is the viscosity of phase j; p_j is the phase pressure; $\bar{g}$ is the gravitational acceleration. In a system of two-phase (oil-aqueous phase) flow, the pressure difference between oil and aqueous phase is the capillary pressure:

$$p_c = p_o - p_a \quad . \tag{7}$$

The effective diffusivity of component i in phase j in porous media, $D_j^{i,e}$, is evaluated with:[5]

$$D_j^{i,e} = \phi^{4/3} S_j^{10/3} \rho_j D_j^i \tag{8}$$

where D_j^i (m^2/s) is the molecular diffusion coefficient of component i in phase j in bulk phase.

Effects of surfactant and salt on flow functions

For an initially oil-wet reservoir, the improved oil recovery by introduction of surfactant into brine is ultimately due to the alteration of flow functions, including capillary pressure, relative permeability and residual saturations. Surfactant, along with the salt (either artificially introduced into or originally resident in the reservoir), can lower the IFT and also alter the wettability of matrix to intermediate-wet or water-wet through removal of oil-wetting components from the matrix surface. IFT and matrix wettability are the factors that control residual saturations, capillary pressure and relative permeability.

A set of models[6] has been proposed by the research group in University of Texas at Austin (called UT models in this paper) to correlate the trapping number with the residual saturation and relative permeability. The trapping number N_T is defined as: [6]

$$N_T = \frac{\left|\overline{\overline{K}} \cdot \left(\nabla p_o + \bar{g}\left(\rho_a - \rho_o\right)\right)\right|}{\sigma} \quad . \qquad (9)$$

It can be seen from Eq. (14) that the trapping number essentially combines the effects of capillary number and Bond number. Note, as proposed by Pope et al.[6], the evaluation of N_T is based on the displaced phase, which is oil phase in the present study.

The following equation is used to correlate residual saturation with the trapping number (Pope et al. [6]):

$$S_{rj} = S_{rj}^{high} + \frac{S_{rj}^{low} - S_{rj}^{high}}{1 + T_j N_T} \qquad (10)$$

where S_{rj} is the residual saturation of phase *j* and T_j is the trapping parameter for phase *j*. The superscript "low" or "high" respectively refers to the parameter value at low or high trapping number. In this equation, S_{rj}^{high} is typically[6] 0. Given the values of S_{rj}^{low} and T_j, which can be obtained by fitting experimental data, Eq. (10) yields the desaturation curve ($S_r - N_T$ curve) that is similar to the CDC curve (capillary desaturation curve) described by Lake.[4] S_{rj}^{low} has the similar meaning as the plateau value of residual saturation as described by Lake[4] and the trapping number plays the role of capillary number. The value of trapping parameter T_j determines the critical trapping number (the trapping number where residual saturation begins to decrease from the plateau value) and the total desaturation trapping number (the trapping number where the residual saturation becomes 0) and it typically has higher value for non-wetting phase and lower value for wetting phase.[6] Note, Eq. (10) has been modified according to the feature of the system under present study, i.e., the hydrocarbon components are simply considered as one pseudo-component.

The effect of wettability is not considered in the trapping number, and therefore it is not incorporated into Eq. (10). In the present study, we use a simple interpolation technique to consider the wettability effect on residual saturation:

$$\frac{S_{rj}^{low} - S_{r,b1}^{low}}{\cos\theta - \cos\theta_0} = \frac{S_{r,b2}^{low} - S_{r,b1}^{low}}{\cos(\pi - \theta_0) - \cos\theta_0}, \qquad (11a)$$

$$\frac{\ln T_j - \ln T_{b1}}{\cos\theta - \cos\theta_0} = \frac{\ln T_{b2} - \ln T_{b1}}{\cos(\pi - \theta_0) - \cos\theta_0} \quad . \qquad (11b)$$

To apply Eqs. (11a) and (11b), first we should have the values of S_r^{low} and T for a pair of base phases, which are represented with subscripts "b1" and "b2" in the equations. Note that we do not distinguish between oil and aqueous phase. Instead, each phase is marked with its contact angle. Without losing generality, let us assume the contact angle for base phase b1 is θ_0, and consequently the contact angle for base phase b2 is π-θ_0. Now the plateau value S_{rj}^{low} and the trapping parameter T_j for phase *j*, of which the contact angle is θ, can be calculated from Eqs. (11a) and (11b), respectively. The values of S_{rj}^{low} and T_j are used to calculate the residual saturation with Eq. (10). Fig. 1 shows a family of desaturation curves ($S_r - N_T$ curves) that are calculated from two base curves for two base phases with contact angle 0 for phase b1 and π for phase b2 (i.e., the medium is totally wetted by base phase b1). For base phase b1, which is the wetting phase, $S_{r,b1}^{low} = 0.2$ and $T_{b1} = 300$. For the non-wetting base phase b2, $S_{r,b2}^{low} = 0.3$ and $T_{b2} = 6 \times 10^4$. The desaturation curves for a pair of phases with wetting phase contact angle $\theta=\pi/3$ and non-wetting phase $\theta=2\pi/3$ can then be obtained through Eqs. (10), (11a), and (11b). As can be seen from Fig. 1, two important features about the wettability effects on CDC curves discussed by Lake[4] have been qualitatively captured. First, the wetting phase has a lower plateau value than the non-wetting phase. For example, the plateau value of the $\theta=\pi/3$

curve (0.225) is lower than that of θ=2π/3 (0.275). Second, the wetting phase has higher critical trapping number and total desaturation trapping number. In Fig. 1, the critical trapping number and total desaturation trapping number for the curve θ=π/3 are around 10^{-4} and 10^{-1}, respectively, and for the curve θ=2π/3, they are 10^{-5} and 10^{-2}. It should be pointed out that Eqs. (11a) and (11b) are just conceptual models for lack of any other models based on experimental data.

In the present study, we use a modified Brooks-Corey model to describe the relative permeability:[4]

$$k_{rj} = k_{rj}^{0}\left(S_j^*\right)^{n_j} \tag{12}$$

where k_{rj}^{0} is the endpoint of the relative permeability k_{rj} and n_j is the exponential parameter that determines the shape of $k_{rj} - S_j$ curve. The normalized phase saturation S_j^* is defined as:

$$S_j^* = \frac{S_j - S_{jr}}{1 - S_{ar} - S_{or}} \quad . \tag{13}$$

The endpoint value k_{rj}^{0} and the exponential parameter n_j for phase *j* are correlated to the residual saturation of phase *j'* through linear interpolation in the UT model. Here phase *j'* is the conjugate phase of phase *j*. For example, in this system, oil is the conjugate phase of aqueous phase and vice versa. Detail investigations of the results in previous studies indicate that the conjugate phase residual saturation may not be a good predictor for k_{rj}^{0} and n_j, especially when wettability alteration is involved (Anderson[7], Fulcher et al.[8], Masalmesh,[9] and Tang et al. [10]). In the present study, let us suppose we have the relative permeability curves measured at a certain trapping number N_{T0} for a pair of base phases with contact angle θ_0 for phase b1 and π-θ_0 for phase b2. We use the following equations to correlate the relative permeability curves with trapping number N_T and contact angle θ:

$$k_{rj}^0 = 1 + \left(k_{r,b1}^0 + \frac{\cos\theta - \cos\theta_0}{\cos(\pi - \theta_0) - \cos\theta_0} \left(k_{r,b2}^0 - k_{r,b1}^0 \right) - 1 \right) \frac{1 + T_{j'} N_{T0}}{1 + T_{j'} N_T} \qquad (14)$$

$$n_j = 1 + \left(n_{b1} + \frac{\cos\theta - \cos\theta_0}{\cos(\pi - \theta_0) - \cos\theta_0} \left(n_{b2} - n_{b1} \right) - 1 \right) \frac{1 + T_{j'} N_{T0}}{1 + T_{j'} N_T} \qquad (15)$$

Eqs. (14) and (15) are just conceptual models that qualitatively capture the typical trends observed in previous studies[7-11] of the effects of capillary number (trapping number in this work) and wettability on relative permeabilities. Note, $T_{j'}$ is the trapping parameter of the conjugate phase of phase *j* and its value is evaluated with Eq. (16b) using the contact angle π-θ, where θ is the contact angle of phase *j*.

Fig. 2 shows a family of relative permeability curves calculated from a pair of base curves with Eqs. (10) – (15). The wetting phase saturation is plotted on x-axis and the relative permeability on the y-axis. As the contact angle θ increases from (wetting) 0 to π, the relative permeability alters along with the residual saturations.

According to the Leverett J-function,[4] the effects of IFT and contact angle on capillary pressure are described with the following equation:

$$p_c = p_{c0}\left(S_a\right) \frac{\sigma \cos\theta}{\sigma_0 \cos\theta_0} \quad . \qquad (16)$$

Here p_{c0} is the capillary pressure between oil and aqueous phase in the base system where aqueous phase contact angle is θ_0 and the IFT is σ_0. It is generally correlated to the normalized aqueous phase saturation S_a. p_c is capillary pressure for the real system where the aqueous phase contact angle is θ and the IFT is σ.

Governing Equations and Numerical Techniques

The mass balance equations for all the components can be written as:

$$\frac{\partial}{\partial t}\left[\phi\left(\rho_a S_a w_a^h + \rho_o S_o w_o^h\right)\right] + \nabla \cdot \overline{F}^h = q^h \qquad (17a)$$

$$\frac{\partial}{\partial t}\left[\phi\left(\rho_a S_a w_a^w + \rho_o S_o w_o^w\right)\right] + \nabla \cdot \overline{F}^w = q^w \qquad (17b)$$

$$\frac{\partial}{\partial t}\left(\phi C^{sf}\right) + \nabla \cdot \overline{F}^{sf} = q^{sf} \qquad (17c)$$

$$\frac{\partial}{\partial t}\left(\phi C^{st}\right) + \nabla \cdot \overline{F}^{st} = q^{st} \qquad (17d)$$

In Eqs. (17a) – (17d), the mass flux term $\overline{F}^i$ is evaluated with Eqs. (1) and (2a) –2(d). We neglect any in-situ source for any component, e.g., the in-situ generation of surfactant, so the source term q^i is determined solely by boundary conditions.

Eqs. (17a) – (17d) are spatially discretized with a finite volume method.[12,13] One-point upstream averaging is employed in the evaluation of phase mobility. The interblock-interphase diffusions are considered with the help of the discretization method of diffusion term described by Pruess et al.[14] This spatial discretization method provides the simulator with flexibility in treatment of 1D, 2D and 3D problems under any coordinate systems (Cartesian coordinates, cylindrical coordinates and irregular coordinates). Backward Euler method is used to approximate the partial derivative of time. This discretization method generates a fully implicit scheme in which 4n nonlinear algebraic equations are solved simultaneously. Here n is the number of grid blocks into which the medium is discretized. For each grid block, four unknowns are solved. Physical appropriateness and numerical stability are two factors that are considered in selection of unknowns. In the present study, we choose the oil phase pressure (p_o), oil phase saturation (S_o), overall surfactant concentration (C^{sf}) and overall salt concentration (C^{st}) as the primary unknowns to be directly solved from the governing equations. Newton-Raphson method

is employed to solve the equation system.[13] A linear solver based on the iterative methods proposed Moridis et al.[13] is used to solve the sparse linear system.

Results and Discussion

Experimental imbibition curves are shown in Fig. 3. It shows cumulative oil recovery (as % OOIP) with the time of imbibition. Initial oil saturation is ~ 72.5 % in each of the cores. Very little oil is recovered (~ 1 % OOIP) from the core immersed in brine. This indicates that the cores used for the study are oil-wet in nature. The other cores were surrounded by surfactant solutions (0.05 wt % Alfoterra surfactants in 0.3 M Na_2CO_3 solution and 1 wt % DTAB solution).

The recovered oil plotted in Fig. 3 is the separated oil in the imbibition cell. A photograph of the imbibition cell is shown in Fig. 4. Since the IFT of the system is low, not all the oil that leaves the core, collects on the top of the cell immediately. Some of the oil remains in the aqueous phase as a macro-emulsion, as shown in Fig. 4. The data that was noted in Fig. 3 did not include the oil trapped in the aqueous macro-emulsion phase. During the initial period of experiments, until about 10 days, the solution surrounding the cores were clear and not much of the oil recovered was trapped in the macro-emulsion form. During the intermediate time, between 10-100 days, the aqueous phase surrounding the cores was found to be brown in nature, with oil trapped in the macro-emulsion form. This amount was later calculated from CT-scan experiments to be about 1-2 ml. After 100 days, there was not much oil recovery from the cores and the settling time for macro-emulsion was shorter than the time-scale of oil recovery, hence the solution started clearing up. At the end of the experiment, most of the oil from the macro-emulsion aqueous phase had segregated to the separated oil phase at the top of the imbibition cell.

We estimate errors of our oil production volume on this basis and add that to the separated oil volume as shown in Fig. 5 for the case of Alfoterra 35 surfactant brine solution. Other anionic surfactants in Fig. 3 show similar error bars. In case of DTAB, there is not much of oil trapped in macro-emulsion phase. Fig. 3 shows that the final oil recovery with surfactant Alfoterra 38 and Alfoterra 35 is around 61% and DTAB gives a recovery of 37%. Final oil recovery from Alfoterra 68 is lower at about 41%. Most of the oil (90% of final recovery) was recovered within 100 days of imbibition, and 50% of the final recovery was produced within 30 days of imbibition.

At the end of the imbibition experiment (with Alfoterra 35 surfactant brine solution), the core was taken and cleaved along the principal directions to visually observe the remaining oil distribution. The image of the cleaved core is shown in Fig. 6, which shows that oil saturation at the top of the core is more than that at the bottom, and the center-saturation is more than the sides. This indicates a possible combination of both gravity-driven and capillarity-driven imbibition process.

Fig. 7 shows the theoretical plot of oil recovery for an entirely gravity-driven process along with the experimentally observed data. $\overline{S}_o$, the average saturation in the core is taken as the remaining oil saturation in the core. S_{or}, residual oil saturation in the core is taken as the oil saturation in the core at the end of the imbibition experiment (adding about 0.5 ml to the recovered oil for the oil that would have recovered had the imbibition experiment been conducted for infinite amount of time). Fig. 7 shows that there is a mismatch between the theoretical and experimentally observed curves during the initial phase of the experiment. This indicates that the process for oil recovery during early times is not entirely gravity-driven. Fig. 7 also shows that for later times, there is a match between the experimental recoveries and the theoretical curve indicating that the process may be gravity-driven for later times.

For the case of very strongly water-wet media, oil-recovery is driven by counter-current imbibition. The dimensionless group derived by Ma et al.[15] is used for estimation of dimensionless time for the experimental data observed in Fig. 3. The experimental data obtained by Ma et al.[15] fitted into a very strongly water-wet (VSWW) curve, which is shown in Fig. 8 for reference. The dimensionless time is a function of the IFT of the system. In case of surfactant brine imbibition, the IFT of the system is a function of surfactant and salt concentrations, which vary with time. For Alfoterra 35 surfactant brine solution IFT of the system changes from an initial value of 30 mN/m to a final value of 0.001 mN/m. Fig. 8 shows plots of oil recovery observed in Fig. 3 with respect to the dimensionless time assuming different IFT's for the system. There is a mismatch between the experimental curve and the VSWW curve for both initial and final IFT of the system. However, there exists an IFT value of 0.01 mN/m for which the experimental curve matches with the VSWW case. It is not clear, how one can anticipate this IFT.

In order to better understand the process of oil recovery from an oil-wet matrix block using surfactants, a 3-D simulator using the numerical models discussed earlier is developed. It is used to simulate the laboratory experiments.

A primary drainage mercury capillary pressure curve was measured for the cores used in the study. The capillary pressure was converted for the gas/water system and is shown in Fig. 9. It could be seen that the carbonate core has a bimodal pore throat size distribution. This capillary pressure curve was further modified for oil-water system using appropriate IFT and contact angles. The end point relative permeabilities were calculated before and after aging for a sample core. These parameters were used in Eqs. (7) – (10) for estimation of relative permeabilities. The exponents for relative permeabilities were used as simulation parameters. The final values used for simulation are given in Table 1.

The partition of each component between aqueous and oil phases was modeled independent of component concentrations. The IFT of the system depends on the surfactant and salt concentrations. This dependence was obtained by fitting a smooth curve through the experimental IFT data obtained by varying the surfactant concentration at 0.3 M Na_2CO_3 solution for water-oil system. The water-oil ratio (WOR) used in this study was fixed at 1:1. The experimental fit is shown in Fig. 10. The IFT is divided into three fits, a straight line fit for low surfactant concentration (<0.01 wt. %), where the IFT is constant at 30 mN/m, another straight line fit for high surfactant concentrations (> 0.035 wt. %) where the IFT is constant at 0.001 mN/m and a third-order polynomial fit for $\ln(\sigma)$ is used for surfactant concentration lying in between the two concentrations. It was assumed that the salt diffusion is much faster compared to the surfactant diffusion in water. Hence, the salt concentration is kept constant at 0.3 M Na_2CO_3. This results in IFT being a sole function of surfactant concentration, and the functional form is shown in Fig. 9. The salt diffusion could be taken into account in the simulator if needed. The effect of WOR on IFT was not incorporated in simulation.

Wettability, measured through contact angle, depends on the surfactant and salt concentrations. This dependence is modeled (for simplicity) similar to IFT behavior, a constant initial contact angle for low surfactant concentrations (<0.01 wt. %), a constant final contact angle for high surfactant concentrations (>0.035 wt. %) and a linear variation of contact angle from the initial value to the final value between the two surfactant concentrations. This is a conceptual model for lack of quantitative model based on experimental data. Experimentally, we know that the initial contact angle is 160^0-180^0. The final wettability of the core is obtained from mineral-scale experiments[3] for the surfactants used, though it is kept as a flexible parameter as the composition of the core is different from the mineral used.

The core is cylindrical in shape and it is assumed to be homogeneous with uniform permeability and porosity. Thus, radial symmetry is assumed for the system. A constant pressure boundary condition is used for the boundaries. A 2-D radial grid is constructed to represent the core as shown in Fig. 11.

The experimental and numerical results are compared in Fig. 5 for Alfoterra 35 alkaline surfactant solution imbibition. It can be seen that there is a match between the experimental data and the numerical simulation. The number of grid blocks used for this simulation is 10 X 40 (10 in radial direction and 40 in the vertical direction). The effect of grid blocks was tested by increasing the number of grid blocks to 50 X 100 and 100 X 100. There was no appreciable difference between the results from 10 X 40 and 100 X 100 grid block simulations. Hence for further analysis the grid blocks used were kept at 50 X 100. The simulation of the oil production also generates in situ distribution of many properties, e.g., the oil-saturation, capillary pressure, IFT, Contact angle, surfactant concentration, etc., with time.

Snap shots of the oil saturation at various times are shown in Fig. 12. At each time, the oil saturation is plotted on the Z-axis, the distance from center of the core as X-axis and the distance from bottom of the core as Y-axis. Since the core is symmetric along the radial direction, profiles along the center of the core to the boundary are plotted. Fig. 12 shows that in the first snap shot, the oil saturation decreases almost uniformly from top to bottom of the core along the sides of the core. This is an indication of counter-current like imbibition. This process is present until the sixth snap shot (t ~24 days). At the end of 24 days Fig. 12 shows a gradient in the oil saturation, with oil saturation being higher at the top of the core than at the bottom. This indicates that the gravitational forces are starting to dominate the process.

Similar snap shots of the capillary pressure, P_c at various times are shown in Fig. 13. At each snap shot the P_c (psi) is plotted on the Z-axis. Fig. 13 shows that in the first snap shot, the

capillary pressure is negative, indicating that the core is oil-wet in nature initially. As surfactant diffuses through the boundary, it alters both IFT and the wettability, thereby changing the capillary pressure, as given by Eq. (16). Fig. 13 shows that P_c reaches a steady value by the end of 18 days. This time also corresponds with the end of counter-current imbibition shown in Fig. 12. By this period of time, P_c is nearly zero.

Fig. 14 shows snap shots of IFT at the same times as in Fig. 12. The IFT (N/m) is plotted on the Z- axis. Similar to Fig. 13, the IFT reaches a steady value by the end of 18 days, which by Eq. 21 results in near-zero P_c shown in Fig. 13. IFT is reduced to a low value by surfactant diffusion, and IFT reduction with surfactant concentration is given in Fig. 9. Fig. 15 shows the change in wettability as measured by contact angle at various times. Wettability is completely altered to water-wet everywhere by the end of 24 days. The contact angle after 24 days of imbibition is 75^o throughout the core, in this example.

The reduction of IFT and change of wettability is caused by an increase in surfactant concentration by diffusion and convection. Fig. 16 shows the surfactant concentration at the same times as in Figs. 13-15. Here, surfactant concentration (as weight fraction in aqueous phase) is plotted on the Z-axis. Fig. 16 shows that the surfactant concentration plateaus after 24 days, hence resulting in the plateaus for wettability, IFT, P_c observed in Figs. 13-15.

Oil recovery from bigger (field-scale) fracture blocks of 1m wide X 1m high to 10m wide X 10 m high were simulated with parameters that matched lab-scale experimental data. The expected recovery from such systems is shown in Fig. 17. All the fracture blocks here are taken to be of the same properties as the core under which experiments were carried out. Fig. 17 shows that 60% recovery takes 30 days in the lab-scale core, 10 years for 1 m X 1 m block and 100 years for a 10 m X 10 m block. The recovery of oil from these cores is controlled by surfactant diffusion. Fig. 17 also shows that the recovery is almost the same for a 10 m wide X 1 m high

and 1 m wide X 10 m high matrix blocks for the first 800 days. Plots of surfactant concentration for these cases also show that by 800 days surfactant reaches a steady value of 0.05 wt % for both these cases. After surfactant has reached a steady value, the mechanism for oil recovery is through gravitational forces. According to Eq. (3), for the same time, as L increases t_{Dg} decreases; this results in lower recovery, E_R. Hence, a smaller block length should have more recovery for the same time. Fig. 17 shows the same, i.e., higher recovery rates for the 10 m wide X 1 m high matrix block compared to 1m wide X 10 m high matrix block.

Effect of wettability alteration was studied by changing the contact angle from the initial value of 180^0 to final values of 180^0(no wettability alteration), 90^0 (intermediate wet), 75^0 (actual wettability), and 0^0 (VSWW). By increasing the extent of wettability alteration it was observed that the recovery increased. Since the process is mostly gravity driven, as residual oil permeability increases (as the block becomes more water-wet), dimensionless time increases, which results in increase of E_R. Hence, for the same time, as the block becomes more water-wet, the recovery increases. It was also seen that in case of no wettability alteration, the final recovery at the end of 100 days was 35% recoverable oil as compared to the experimental case of 75% recoverable oil, indicating again that wettability alteration is an important parameter for surfactant selection.

Since most carbonate reservoirs do not have as high a permeability as 150 mD, simulations were carried out to see the time for oil recovery in tighter reservoirs. The effect of permeability on oil recovery for two different size matrix blocks is shown in Fig. 18. For the same size (lab-scale core), a 150 mD core gives 60% recovery in 30 days, and 7 mD cores gives the same recovery in 400 days. There is almost a linear relationship between the recovery and the permeability indicating that the process may be mostly gravity-driven).

Technology Transfer

We have written a paper, SPE 93009, for presentation in December, 2005. We have collaborated with Oil Chem, Stepan, and Sasol for surfactants.

Conclusions

We have developed a 3-D flexible grid finite volume simulator for 2-phase salt/water/oil/surfactant system. Simulator is capable of analyzing changes in wettability and IFT as functions of surfactant and salt concentrations in both phases, thereby changing relative permeabilities, residual saturations and the capillary pressure. The simulator matches the experimentally observed imbibition data, and then it is used for scale-up. Based on the experiments and the simulations the following can be concluded. Laboratory scale surfactant brine imbibition experiments give high oil recovery (35-62% OOIP) for initially oil-wet cores through wettability alteration and IFT reduction (Task 4). Core-scale simulation results match those of the experiments. In-situ distributions observed through simulation indicate that surfactant distribution is the rate limiting step. Initial capillarity-driven imbibition gives way to a final gravity-driven process. The capillary pressure needed for counter-current imbibition goes to near zero because of low interfacial tension before less than 30% oil recoverable is recovered. The rest of the oil is recovered through gravitational forces. As the matrix block height increases, surfactant alters wettability to a lesser degree, or permeability decreases, oil production rate decreases. (Task 5)

Plans for Next Reporting Period

- Simulation (Task 5)

References

1. Bragg, J. R. et al.: "Loudon Surfactant Flood Pilot Test," SPE/DOE 10862, SPE/DOE 3rd Joint Symposium on EOR, Tulsa, April 4-7, 1982.
2. Spinler, E. A. et al.: "Enhancement of Oil Recovery Using Low Concentration Surfactant to Improve Spontaneous or Forced Imbibition in Chalk," SPE 59290, SPE/DOE Improved Oil Recovery Symposium, Tulsa, April 3-5, 2000.
3. Seethepalli, A., Adibhatla, B., and Mohanty, K.K.: " Physicochemical Interactions During Surfactant Flooding of Fractured Carbonate Reservoirs", *SPEJ*, **9**(4), 411-418 (December, 2004).
4. Lake, L. W.: *Enhanced Oil Recovery*, Prentice-Hall Inc. Upper Saddle River, NJ. (1989).
5. Pruess, K. and Moridis, G. TOUGH2 User's Guide, Version 2.0. LBNL-43134. Lawrence Berkley National Laboratory, University of California, Berkley, California 94720, 1999.
6. Pope, G. A., Wu, W., Narayanaswamy, G., Delshad, M., Sharma, M. M. and Wang, P.: "Modeling Relative Permeability Effects in Gas-Condensate Reservoirs with a New Trapping Model," *SPE Reservoir Eval. & Eng.,* **3** (2), 171-178 (2000).
7. Anderson, A. G.: "Wettability Literature Survey-Part 5: The Effects of Wettability on Relative Permeability," *J. Petroleum Technology,* 1453-1468 (November, 1987).
8. Fulcher Jr, R. A., Ertekin, T. and Stahl, C. D.: "Effect Of Capillary Number and Its Constituents on Two-Phase Relative Permeability Curves," *J. Petroleum Technology,* 249-260 (February, 1985).
9. Masalmesh, S. K.: "The Effect of Wettability on Saturation Functions and Impact on Carbonate Reservoirs in the Middle East," Proceedings of the 10th International Petroleum Exhibition and Conference. SPE 78515, 13-16 October, Abu Dhabi, 2002.

10. Tang, G. and Firoozabadi, A.: "Relative Permeability Modification in Gas/Liquid Systems through Wettability Alteration to Intermediate Gas Wetting," *SPE Reservoir Eval. & Eng.,* **5**, 427-436 (2002).
11. Bardon, C. and Longeron, D. G.: "Influence of Very Low Interfacial Tensions on Relative Permeability," *SPEJ,* **20**, 391-401 (October, 1980).
12. Heinemann, Z. E., Brand, C. W., Munka, M. and Chen, Y. M.: "Modeling Reservoir Geometry with Irregular Grids," SPE 18412, Proceedings of the SPE symposium on reservoir simulation, Houston, TX, 6-8 February, 1989.
13. Moridis, G. J. and Pruess, K.: "T2SOLV: An enhanced package of solvers for the TOUGH2 family of reservoir simulation codes," *Geothermics*, **27** (4), 415-444, 1998.
14. Press, W. H., Teukolsky, S. A., Vetterling, W. T. and Flannery, B. P.: Numerical Recipes in Fortran 77: the Art of Scientific Computing. 2nd Ed. Cambridge University, Cambridge, UK, 1992.
15. Ma, S., Zhang, X., and Morrow, N.R.: "Influence of Fluid Viscosity on Mass Transfer between Rock Matrix and Fractures," J. *Can. Pet. Tech.*, **38**, 25-30 (1999).

Table 1	
Properties of the limestone core used for imbibition	
Length (cm)	15
Diameter (cm)	3.85
Porosity	22.0 %
Permeability(mD)	150
S_{or}	25.0 %
S_{wr}	27.5 %
k_{rwet}^{0}	0.1
n_{wet}	4.5
$k_{r.nw}^{0}$	0.9
n_{nw}	2.25

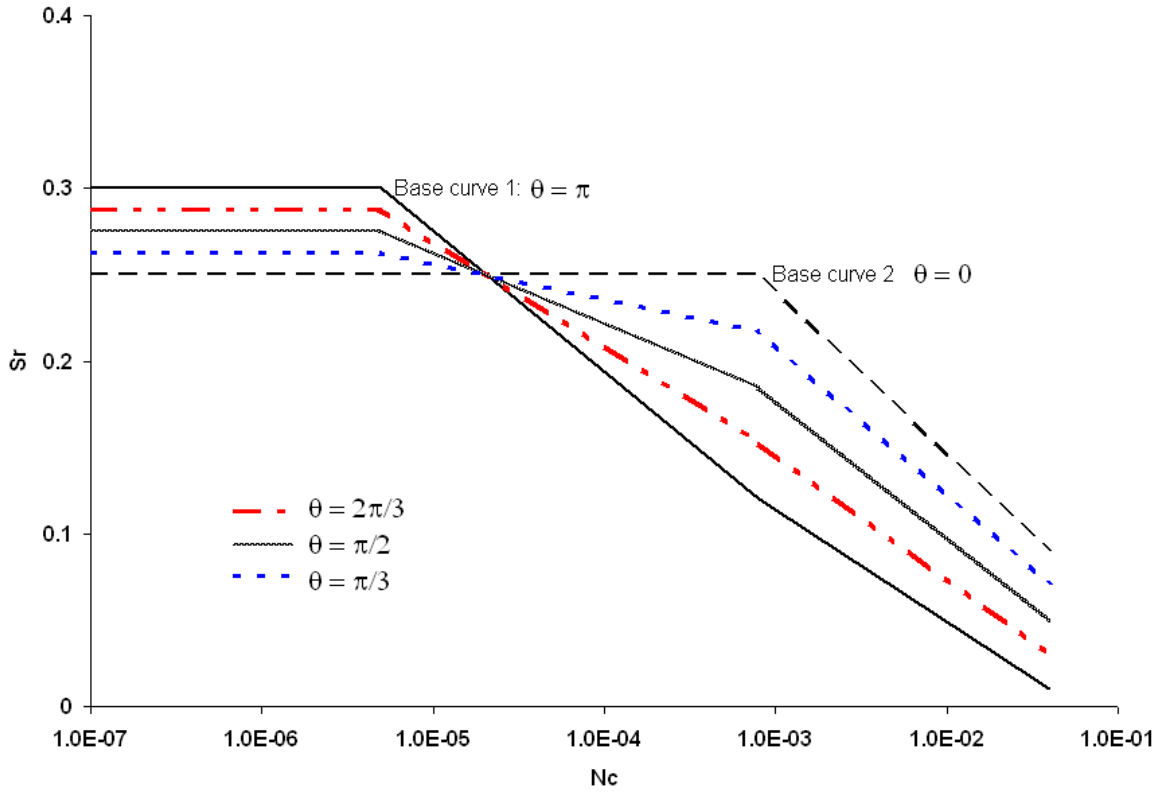

Fig. 1: Capillary desaturation curve as function of wettability

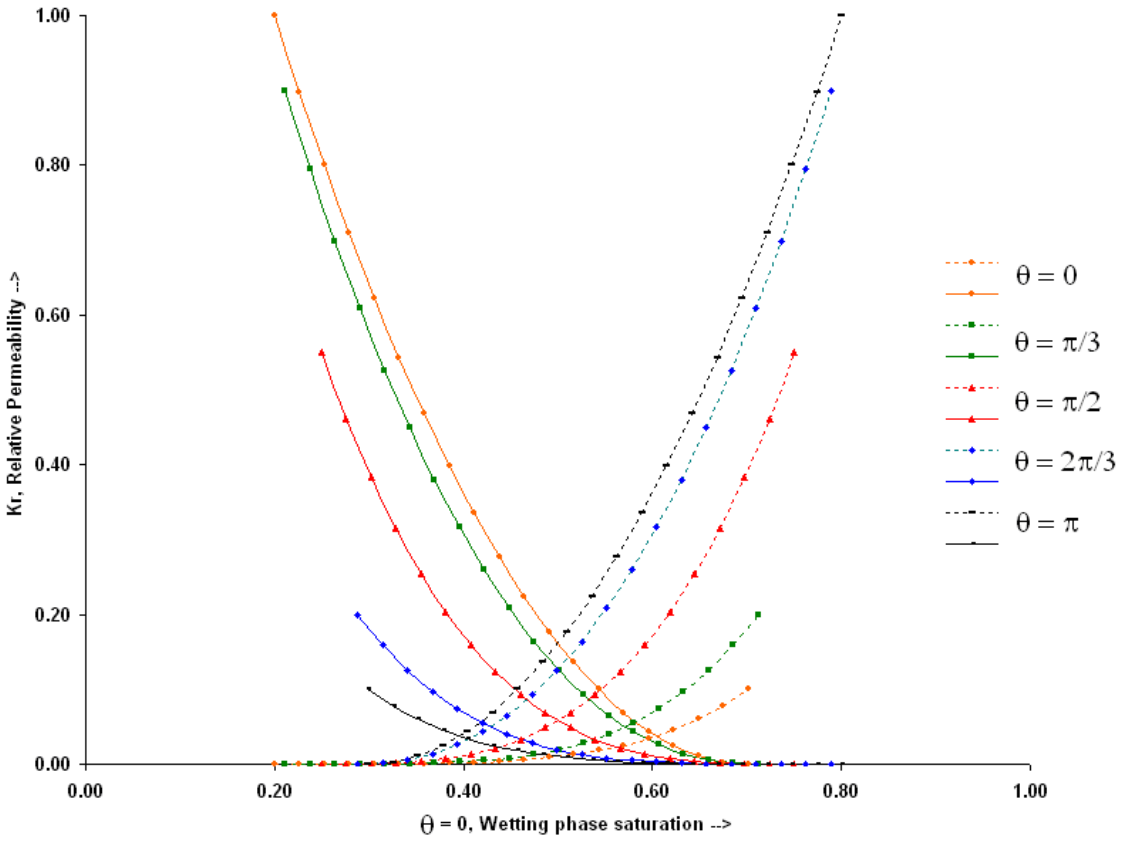

Fig. 2: Relative permeability variation as a function of contact angle

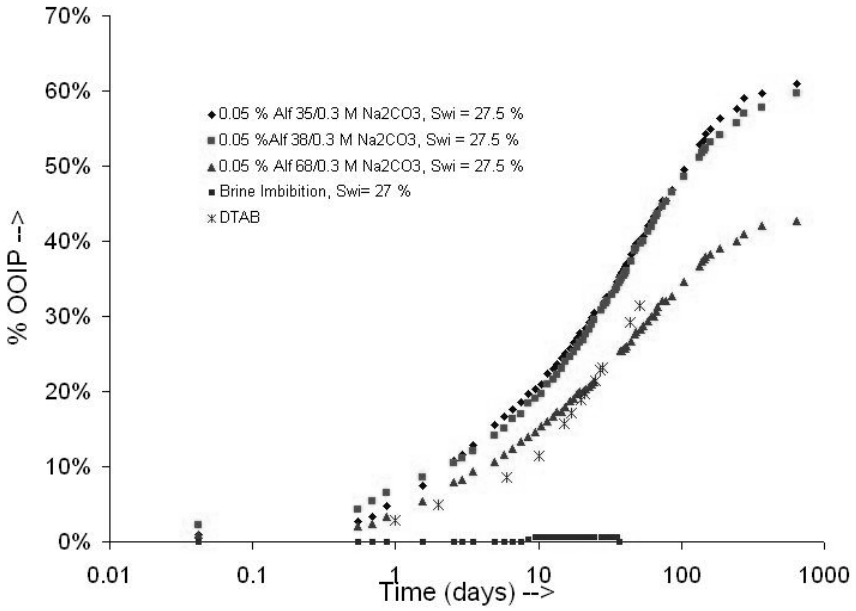

Fig. 3: Oil (separated) production for the surfactant brine imbibition in initially oil-wet cores.

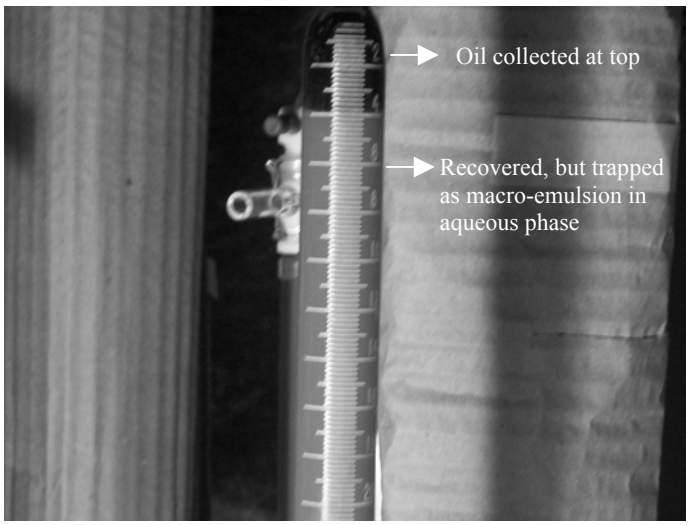

Fig. 4: Oil collected at the top of the imbibition cell

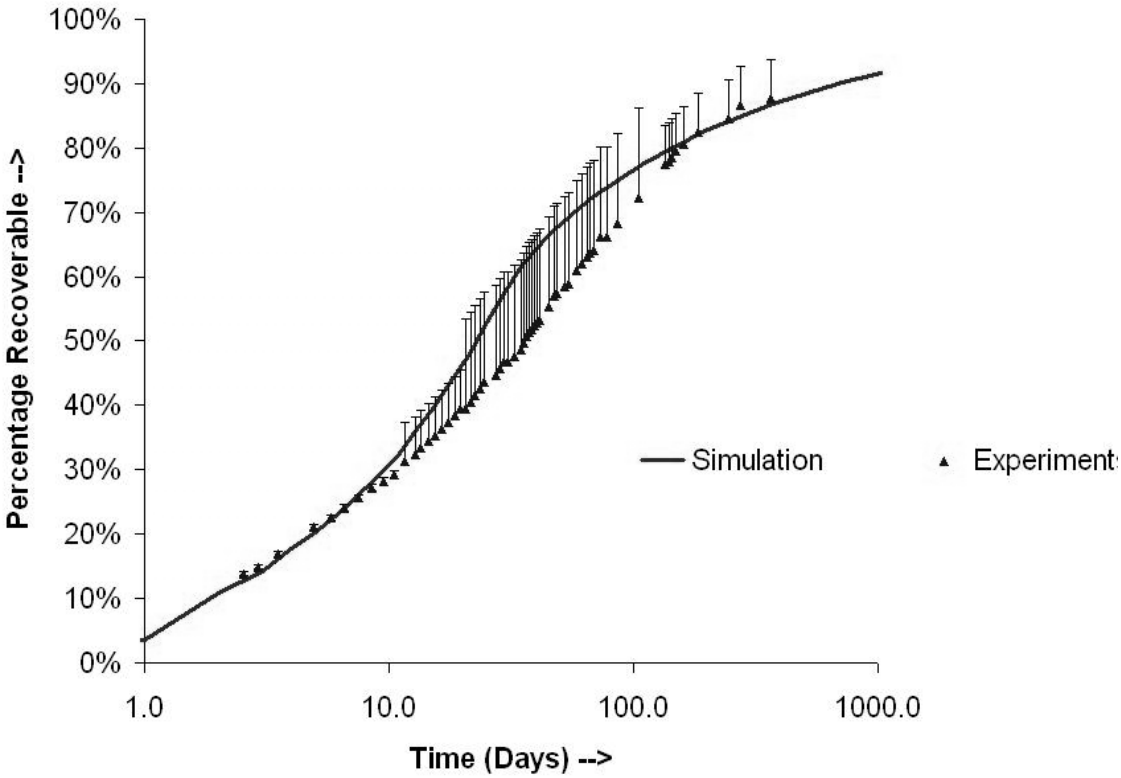

Fig. 5: Oil recovery comparison for the core surrounded by Alf-35 surfactant and 0.3 M Na_2CO_3 solution

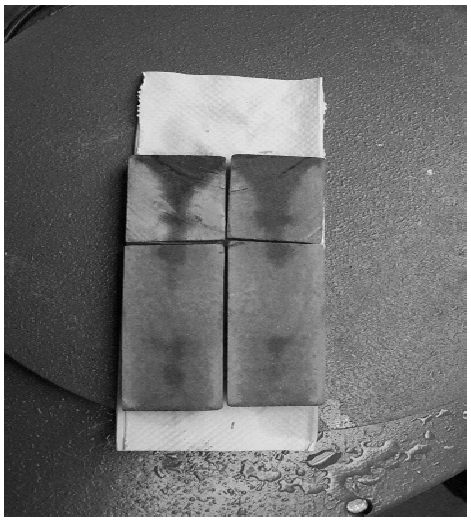

Fig. 6: Cleaved section of core at the end of imbibition

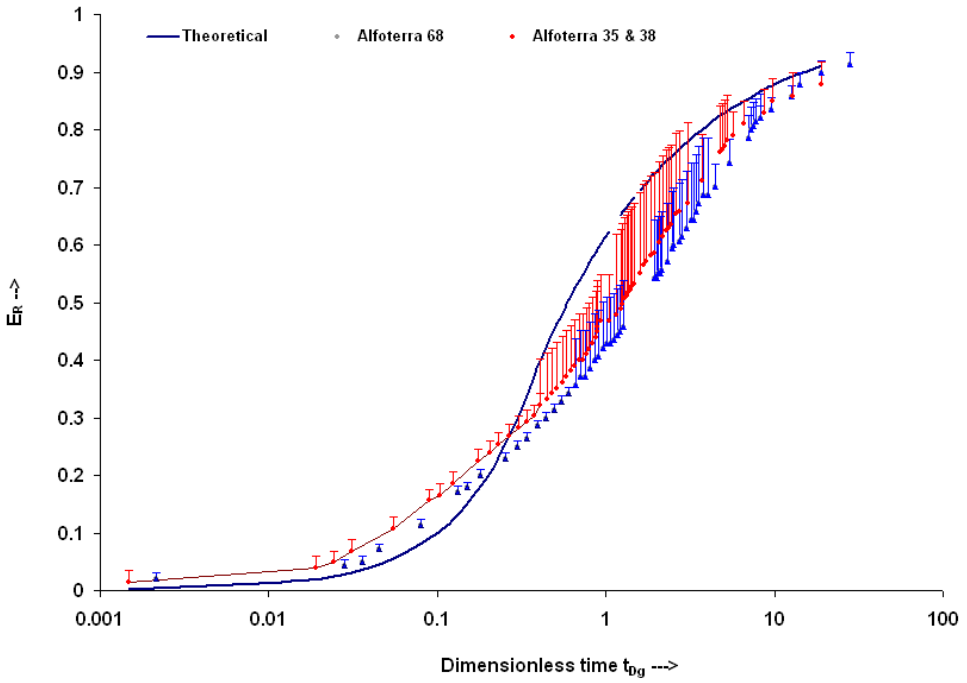

Fig. 7: Comparison of experimental results with theoretically predicted curve for gravity drainage

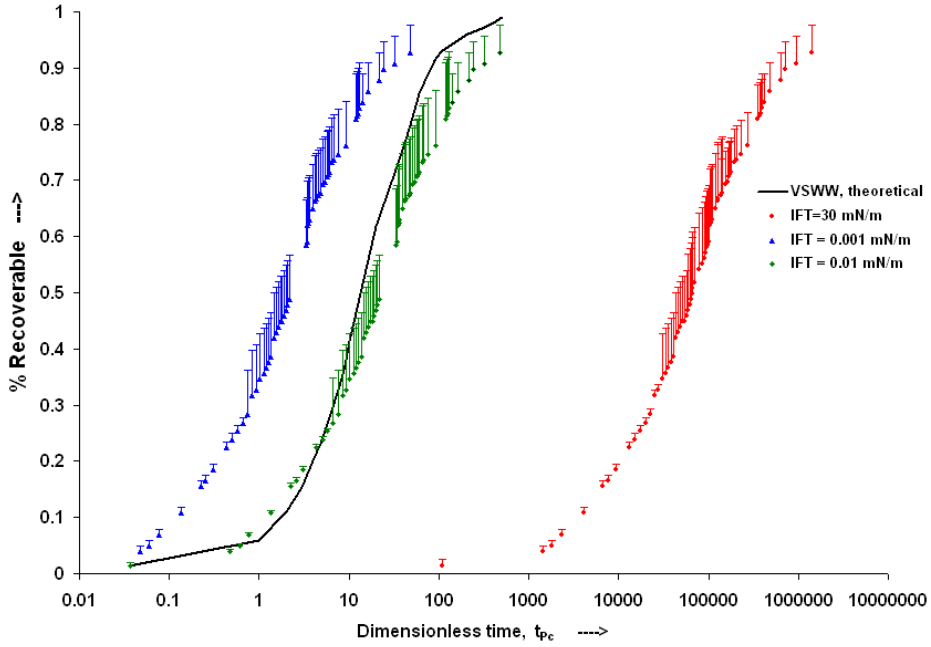

Fig. 8: Comparison of the experimental results with theoretically predicted capillarity-driven strongly water-wet curve

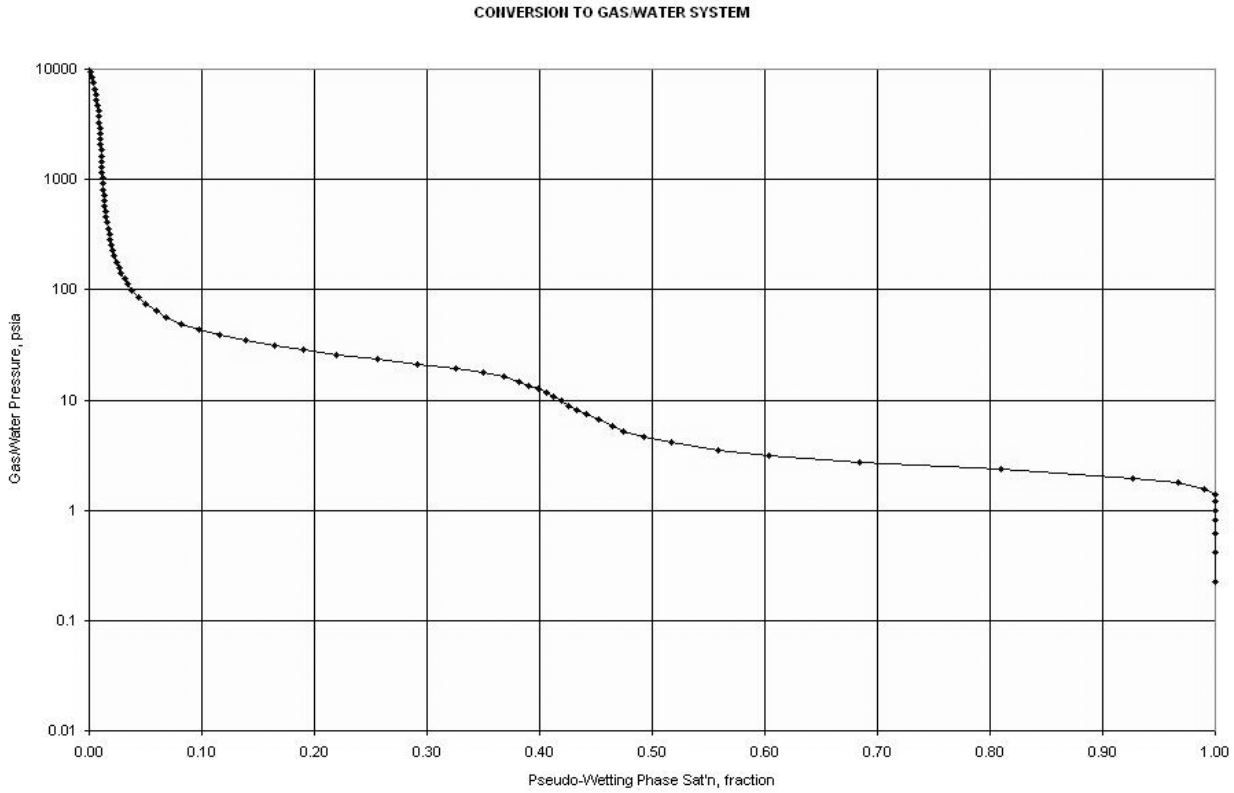

Fig. 9: Primary drainage capillary pressure curve for the cores used in the experiment.

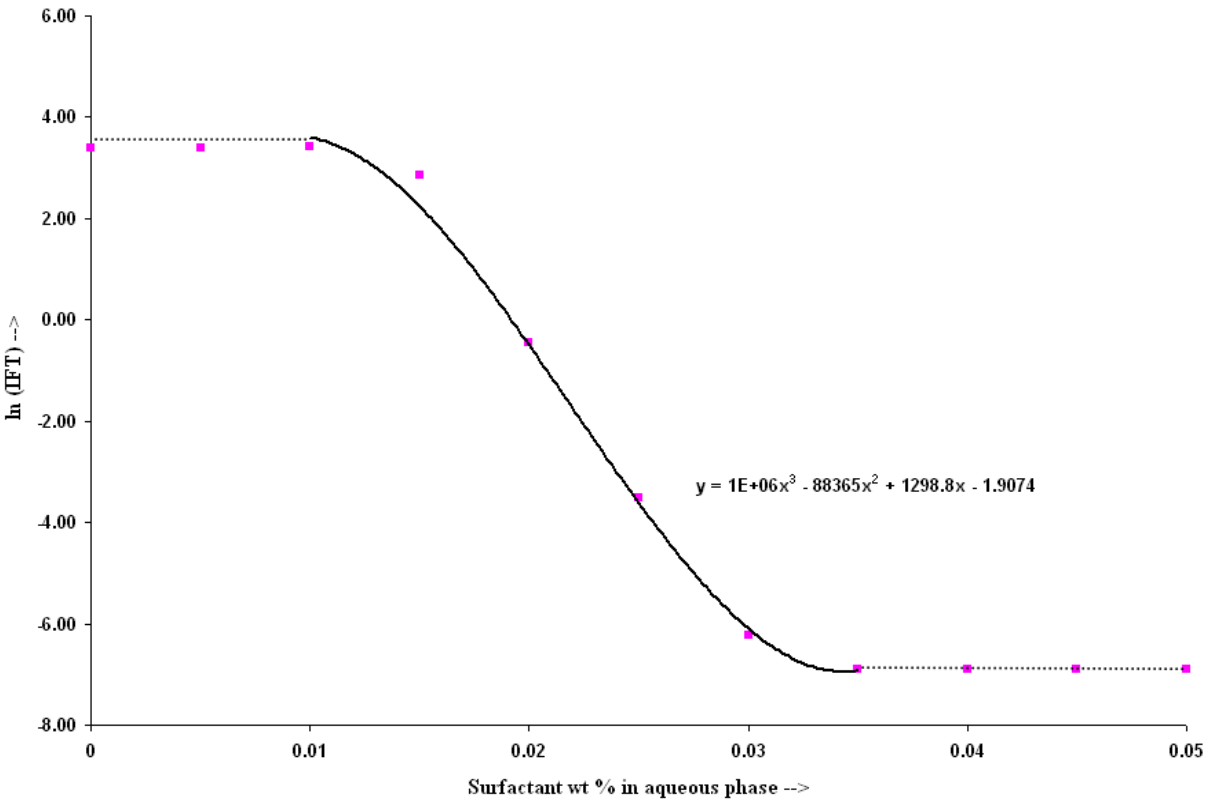

Fig. 10: IFT as function of surfactant concentration at 0.3 M Na_2CO_3 with numerical fit.

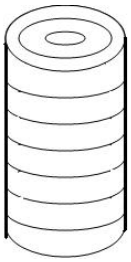

Fig. 11: Simulation grid structure for a cylindrical core

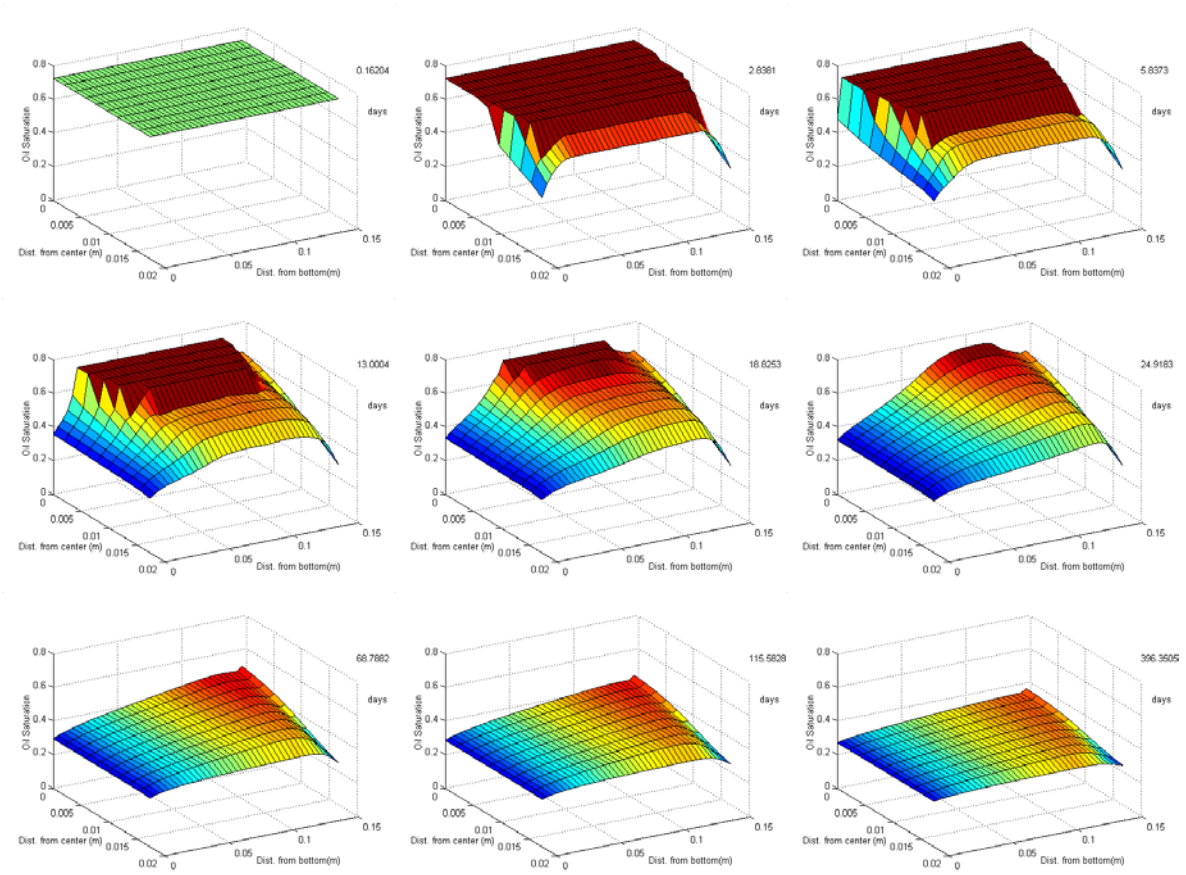

Fig. 12: Oil Saturation at various times, t=0.16, 2.8, 5.8, 13, 18.8, 24.9, 67, 115, 395 days from top left, row-wise. X-axis is radial distance from center, Y-axis is distance from bottom, and Z-axis is the saturation of oil.

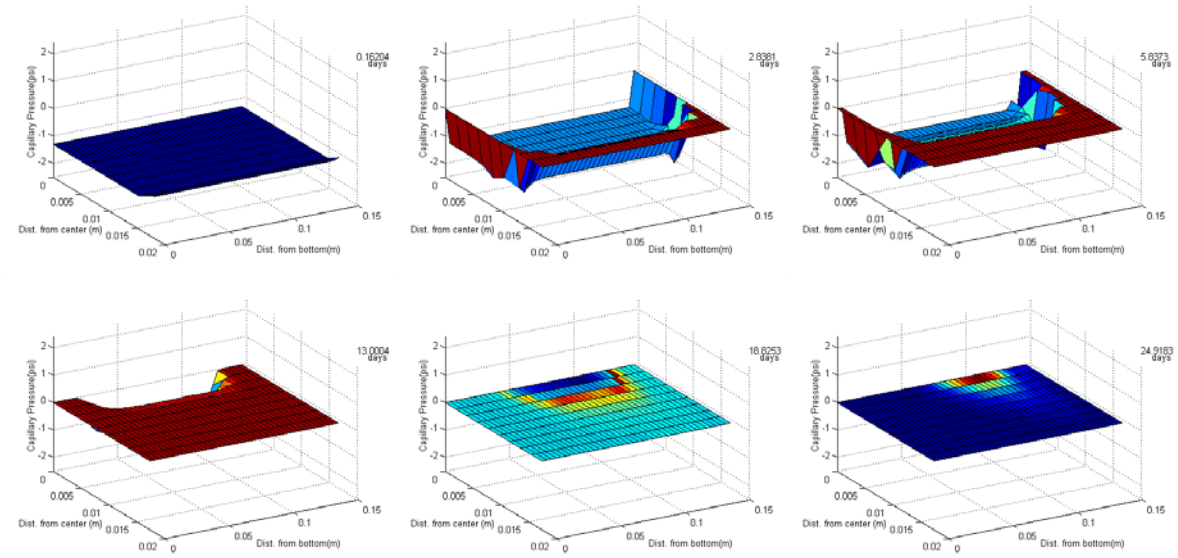

Fig.13: P_c at various times, t = 0.16, 2.8, 5.8, 13, 18.8, 24.9 days from top left, row-wise. Z-axis is the P_C. X and Y axes are the same as in Fig 12. System reaches P_c=0, after 18 days of imbibition.

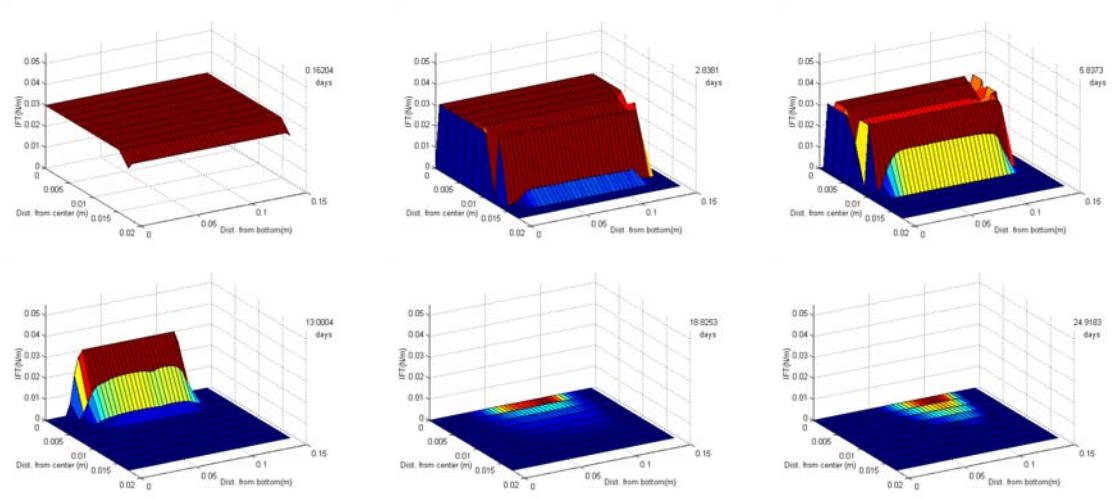

Fig. 14: IFT at same times as in Fig. 13. Z-axis is IFT (N/m).

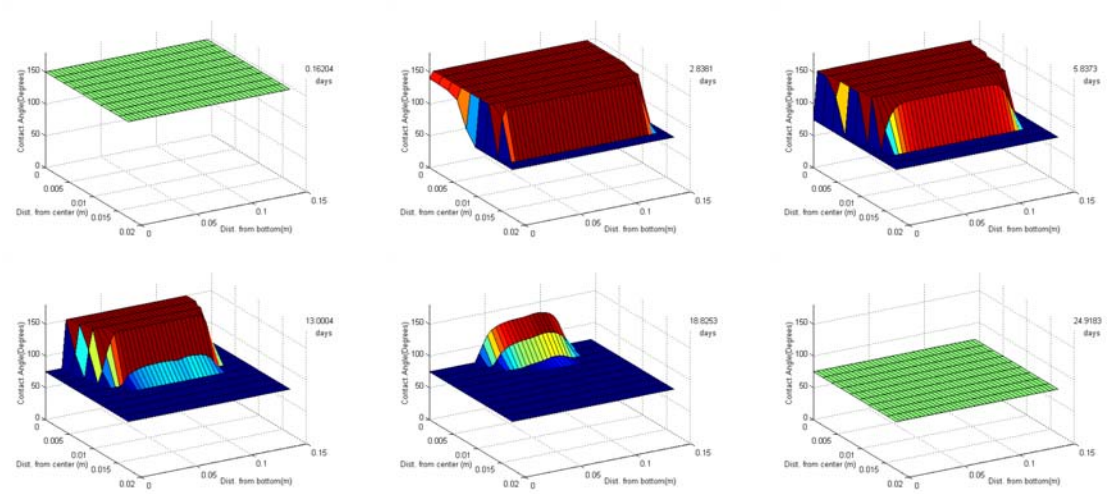

Fig. 15: Contact angle at same times as in Fig. 13. Z-axis is contact angle (^{o}).

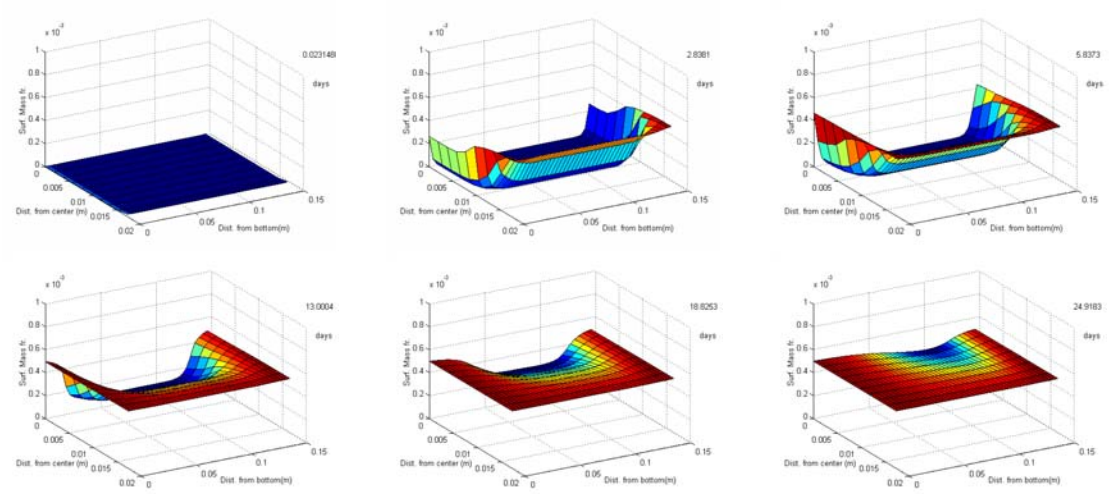

Fig. 16: $C_{surfactant}$ at various times, t = 0.16, 2.8, 5.8, 13, 18.8, 24.9 days from top left, row-wise. Z-axis is the surfactant concentration in weight fraction in aqueous phase. System reaches steady value of 0.05 weight % in 24 days.